Capillaric-Field Effect Transistors

Claude Meffan[*ag] , Julian Menges[abd] , Fabian Dolamore[bd], Daniel Mak[ad], Conan Fee[cd], Renwick C.J. Dobson[def] and Volker Nock[*adf]

a. Department of Electrical and Computer Engineering, University of Canterbury, Christchurch 8041, New Zealand

b. School of Biological Sciences, University of Canterbury, Christchurch 8041, New Zealand.

c. School of Product Design, University of Canterbury, Christchurch 8041, New Zealand.

d. Biomolecular Interaction Centre, School of Biological Sciences, University of Canterbury, Christchurch 8041, New Zealand

e. Department of Biochemistry and Molecular Biology, Bio21 Molecular Science and Biotechnology Institute, University of Melbourne, Victoria 3010, Australia

f. The MacDiarmid Institute for Advanced Materials and Nanotechnology, Wellington 6140, New Zealand

g. Department of Micro-engineering, Kyoto University, 615-8540, Kyoto, Japan

Abstract

Controling fluid flow in capillaric circuits is a key requirement to increase their uptake for assay applications. Capillary action *off*-valves provide such functionality by pushing an occluding bubble into the channel using a difference in capillary pressure. Previously, we utilised the binary switching mode of this structure to develop a powerful set of fundamental fluidic valving operations. In this work we provide evidence that these structures are in fact functionally complementary to electronic Junction Field Effect Transistors and thus warrant the use of the new term of capillaric-Field Effect Transistor to describe these types of valves. To support this conclusion, we present a theoretical description, experimental characterisation, and practical application of analog flow resistance control. In addition, we demonstrate that the valves can also be re-opened. These are two key capabilities previously missing for a full analogy to electronic transistors. We show modulation of the flow resistance from fully open to pinch-off, determine the flow rate – trigger channel volume relationship and demonstrate that the latter can be modeled using Shockley's equation for electronic transistors. Finally, we provide a first example of how the valves can be opened and closed repeatedly.

1. Introduction

Capillarics is a growing field within microfluidics that offers great potential for point-of-care (PoC) testing due to its use of capillary action driven, pre-programmed chips that can be fabricated in large numbers.[1-3] Without the need for auxiliary pumping and valving operations, complex operations can be scaled down easily, offering lab-on-a-chip level functionality in cheap, portable, and user friendly devices.[4,5] These advantages have led to capillarics being used for a wealth of new applications in recent years, in particular in the biosensing space.[6-18] One fundamental requirement for the fully autonomous operation of capillaric circuits continues to be the availability of basic valving operations that do not need any external power source. Until recently, this was limited to two-level trigger valves[1,2,19] or externally controlled valves.[20,21]

Expanding available valving options, we recently reported a capillary action *off*-valve structure which uses capillary pressure to inflate an occluding air bubble into a microfluidic channel, thus preventing further flow.[22] While trapped bubbles have been used for various applications in pressure-driven microfluidics[23], including to alter flow dynamics, mixing[24], and to realize hydraulic capacitors[25], they have not yet been extensively used in capillarics. To fill this gap, we demonstrated autonomous capillary-action fluidic valving, with no need for external instrumentation, and a variety of fundamental valving operations, including use to provide feedback, metering and logic operations.[26] As eluded to in our previous work, the *off*-valves hold the potential for more transistor-like switching and resistance tuning. This stems from the construction and operational principle of the *off*-valve, which are shown in Fig. 1 in comparison to an electronic Junction Field Effect Transistor (JFET).[27,28] In this communication we report the demonstration that the *off*-valve can indeed be used to control the flow resistance of the main channel in non-binary ways and that it can also oscillate, similarly to a JFET. The particular operating principle of the *off*-valve is different to that of other fluidic transistors, such as the pressure-controlled Field Effect Transistor (pFET)[29], in that it acts on a continuous liquid volume and actually modulates the volume flow of this. We thus propose the introduction of the new term capillaric-Field Effect Transistor (cFET) for the *off*-valve to reflect this new functionality, the role of the junction and similarity to electronic JFET and pFET.

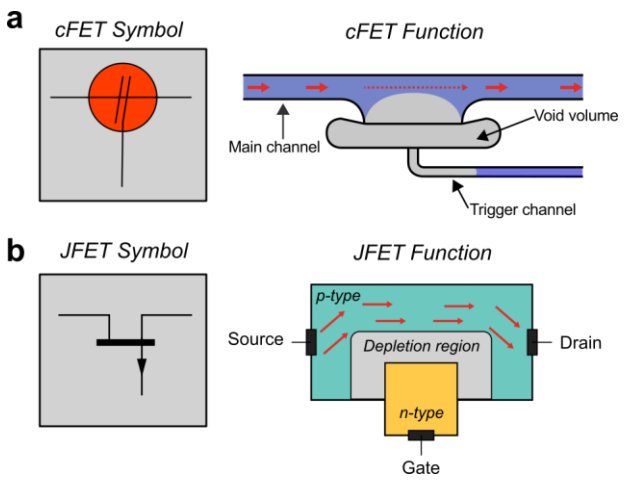

Fig. 1 Construction and operational principle of the off-valve as capillaric-Field Effect Transistor (cFET). a Circuit symbol, structure and operational principle of the capillaric-FET. An air bubble is expanded into the main channel via a trigger channel to control flow resistance in the former. **b** Symbol and basic operation of an electronic JFET. In this structure the depletion region reduces the cross-section of the conducting channel, restricting electrical current flow. Despite different physical mediums, the similar geometries of these structures allow for significant theoretical and operational overlap.

As shown in Fig. 1a, the *off*-valve/cFET device consists of three structures: the main channel, a trigger channel, and a void volume. The main channel is the fluidic channel being switched, whereas the trigger channel is a smaller channel providing the capillary pressure used for switching. This pressure is delivered via the void volume, which acts as an isolation structure, insulating the main and trigger channels from each other. During *off*-valve operation, liquid wets through the main channel and across the large opening at the interface with the void volume. As indicated in Fig. 1a, the liquid does not flow into the void volume because of the height difference between the two structures and the sharp geometric edge created by this.[30] This leaves a large, low pressure meniscus spanning the opening. When the trigger channel subsequently fills with liquid, air is displaced. The high-pressure trigger channel meniscus forces the low-pressure main channel meniscus into the main channel. This locates an occluding bubble into the main channel - restricting fluid flow through it. When the occluding bubble reaches the opposite wall of the main channel, fluid flow is completely pinched off.

For comparison, an electronic JFET and its operation principle are also shown in Fig. 1b. Both are three terminal devices, which feature a conductive channel, either liquid or electronic. In case of the electronic JFET, a field-effect applied from a control terminal forces a non-conductive volume into the main channel, reducing its cross-sectional area and increasing its resistance. The electric field depleting the semiconductor of p-type charge carriers in the JFET is comparable to the pressure field created by the trigger channel depleting the main channel of fluid in the cFET.

Despite the conceptual symmetry an *off*-valve has with an electronic JFET, it was decided that it did not meet the requirements for full transistor functionality[27] on two main points. Firstly, the valve was not demonstrated to control flow resistance of the main channel in non-binary ways. Secondly, the structure could not oscillate – it could not be re-opened, and then be re-closed. This seeming lack in functionality is intrinsic to capillary devices, as all operations are hardwired for single use.[31] There may be options to bypass this in future setups, but the number of uses will always be limited to the operations hardwired on the chip.

The key argument supporting that the capillary *off-valve* is a transistor, is that it can exert a *continuous* controlling force on the flow resistance of the main channel using a third (fluidic) terminal. The ‘exerting control’ property in electrical transistors is the transfer-conductance, or the *transconductance* of the device.[27] This concept defines the size of the conductance change of the main channel, which is transferred or exerted from the control terminal using solid-state geometry. The transconductance of a capillary *off*-valve can be experimentally determined and used with existing transistor models to predict behaviour.

In the following, we develop a theoretical model for the closing dynamics of the *off*-valve, show the flow-rate-volume relation, adapt the JFET Shockley equation[27,28] for this capillary structure, demonstrate that a capillary *off*-valve can be re-opened, and discuss the relevance and future applications for capillary transistors. We use the term capillaric-FET, or cFET, from this point to reflect this new evidence.

The theoretical basis for many capillary action structures is the Young-Laplace equation (Eq. 1). This describes a general capillary pressure, P_{cap}, created by a liquid-gas interface.[32] In this work, the Young-Laplace equation for square-microchannels and for principal meniscus curvature are used:

$$p_{cap} = -\gamma\left(\frac{cos\theta_{roof} + .cos\theta_{floor}}{h} + \frac{cos\theta_{left} + cos\theta_{right}}{w}\right) = -\gamma\left(\frac{1}{R_{horizontal}} + \frac{1}{R_{vertical}}\right) \quad (1)$$

where γ is the liquid surface tension, θ the water contact angle with the channel roof, floor, and left and right walls respectively, h the height of the microchannel, w the width of the microchannel, and $R_{horizontal}$, and $R_{vertical}$ are the principal radii of curvature of the meniscus. This equation is used in the following section to derive a model for the transient dynamics of the cFET.

2. Results

Transient dynamics of the cFET

It is important to develop a thorough theoretical understanding for the dynamics of the cFET to develop a model for its analog functional modes and behaviour throughout closing. For this we initially focus on the actuation speed of the cFET. The proposed dynamical model follows the convention of first-order electrical systems analogies. This approach is well established in both general microfluidics[32] and capillaric circuits.[33] Figure 2 shows the proposed model, overlaid on a rendering of the *off*-valve/cFET.[22]

In this model there are two capillary pressures, symbolically modelled in Fig. 2a as voltages. The first pressure is created by the meniscus in the trigger channel, P_{tr}. This is a constant value and can be calculated using the Eq. 1. The second pressure, P_m, is created by the meniscus that spans the large opening at the edge of the void volume. This pressure is not constant, but rather a function of displaced trigger channel volume, V. The magnitude of this pressure will increase at higher trigger channel displacements. Due to the complex geometry of the main channel, the main channel pressure cannot easily be calculated. However, the form of the response is expected to be similar to an exponential approach, as shown in Fig. 2b.

There are four flow resistances which restrict fluid flow in this model. These represent the liquid and gas contributions for both the trigger channel and body of main channel. Due to its large width, height, and short length compared to the trigger channel - the main channel flow resistances are assumed to be negligible. As such we simplify the hydraulic resistances to the two fluid resistances of the trigger channel, now labelled as R_{gas}, and R_{liquid}.

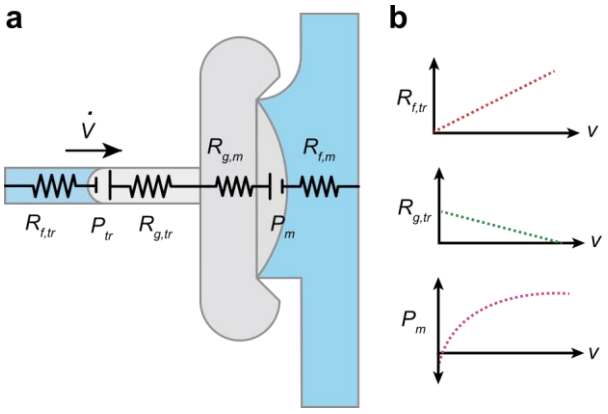

Fig. 2 Electrical analogy model, and fluidic and gas resistances of the cFET. a Dynamical electrical analogy model for the closing behaviour of a cFET. The model is overlaid on a representation of the physical structure to show the physical quantities they represent. Two capillary pressures, P_{tr} and P_m, and four resistances, $R_{f,tr}$, $R_{g,tr}$, $R_{g,m}$ and $R_{f,m}$, are used to model the cFET behaviour. **b** The fluid and gas resistances, and the main channel capillary pressure change as a function of the displaced trigger channel volume. Note: These graphs show the expected form of these properties only.

It is worth noting that these flow resistances do not stay constant over the closing of the device. As the trigger channel fills with liquid, air is displaced, causing the liquid flow resistance to increase and the gas component to decrease. While for most cases, the air flow resistance is negligible compared to the liquid component, it cannot be neglected. If it was removed, then the total flow resistance would become 0 at $t = 0$. Using the two capillary pressures, and the two trigger channel flow resistances, we can describe the flow rate in the trigger channel using a differential equation as,

$$\dot{V} = \frac{P_{tr} - P_m(V)}{R_{liquid}(V) + R_{gas}(V)}, \qquad (2)$$

where $\dot{V}$ is the first derivative of volume with time, P_{tr} the pressure of the trigger channel, $P_m(V)$ the pressure of the main channel as a function of displaced trigger channel volume, $R_{liquid}(V)$ the fluid resistance of the trigger channel as a function of displaced trigger channel volume, and $R_{gas}(V)$ the fluid resistance of the gas in the trigger channel as a function of volume. Equation 2 is linearly separable, and so it should be possible to solve the differential equation analytically. However, as the analytical form of the main channel capillary pressure is not currently known, we proceed numerically in the following.

In our previous work[22], the closing time of the *off*-valve (cFET) was measured by the time taken for the occluding bubble to touch the wall of the main channel. The volume of air required to do this was termed the "pinch-off volume", V_p. Therefore, the closing time of the valve is the time to displace V_p through the trigger channel. With initial conditions $V(0) = 0$, $\dot{V}(0) = 0$, we can express the closing time for a cFET as,

$$t_{close} = \int_0^{V_p} \frac{R_{liquid}(V)+R_{gas}(V)}{P_{cap,tr}-P_{main}(V)}\, dV \qquad (3)$$

Many of the parameters in Eq. 3 are known or can be calculated. The hydraulic resistance of a square cross-section channel, R_h, can be calculated by the well-known empirical relation[34],

$$R_h \approx \frac{12\mu L}{wh^3\left(1-0.63\frac{h}{w}\right)}, \qquad (4)$$

where μ is the liquid viscosity, L the length of the channel, w the channel width, and h the channel depth. This can be used to calculate the trigger channel fluid resistances, R_{gas}, and R_{liquid}. P_{tr} is defined by the trigger channels height, depth, and contact angle through the Young-Laplace equation. However, the pinch-off volume, V_p, and the main channel capillary pressure are not known and difficult to determine analytically.

To obtain values for these, a Polymethylmethacrylate test chip was designed, fabricated and tested (ESI, Fig. S1) according to methods described in detail in our previous work.[22,26] As per its design, this chip systematically varied the trigger channel volume of a number of cFETs to place the occluding bubbling in a range of states. These states are essentially stable snapshots of the meniscus at discrete time points throughout the complete closing of the cFET. A complete CAD rendering of the design is shown in Fig. 3 (CAD files provided in the ESI), with the inset depicting a close-up of the trigger channel structures. The variation in the channel length, and therefore volume, places the cFETs in a controlled range of states between completely open and completely closed. A full range of resultant bubble states can be seen in Fig. 4a. These states can in turn be used to determine both the pinch-off volume and the main channel capillary pressure. The pinch-off volume is estimated by visually inspecting when the bubble touches the opposite channel wall. In the case of the test chip, the trigger channel volume for which the bubble touches the main channel wall was determined as 25.7 *nL*. This method of determining the pinch-off volume, is limited by the how accurately the point when the bubble touches the wall can be observed. In our previous work[22], the ability to precisely determine this point was a limitation due to the resolution and frame rate of the recorded video. In this experiment, the resolution is still a limitation, however because the displaced volume is static, the frame-rate error can be disregarded.

The main channel capillary pressure on the other hand has a vertical and horizontal component. The vertical component is defined by the height and contact angle of the main channel and is constant throughout the cFETs closing. Meanwhile, the horizontal component can be calculated by finding the radius (principal radii) of the bubble in each sub-image of Fig. 4a - up until the pinch-off volume. Figure 4b shows the radii of the occluding bubbles plotted against the trigger channel volumes that created them, up until the pinch-off volume. An example of a circular arc fitted to the extracted meniscus shape is shown as inset in Fig. 4b. In most cases an excellent fit was achieved with a mean square error of less than 1 pixel. There were however, two large outliers in the recorded data indicated in Fig. 4b as red triangles.

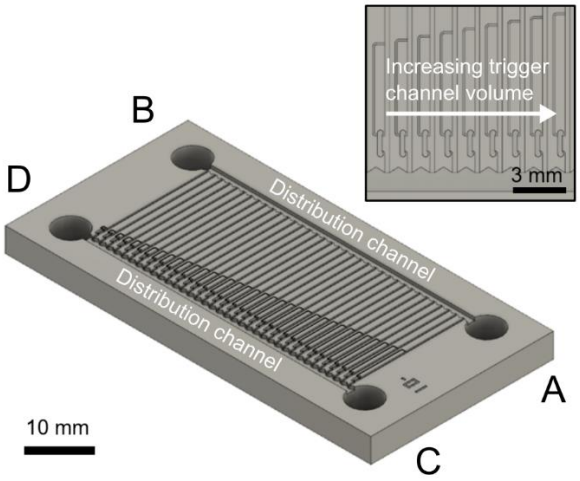

Fig. 3 CAD rendering of the analogue resistance mode test chip. The device was fabricated using micro-milling in Polymethylmethacrylate, as reported previously[22], and consisted of 36 cFET structures arranged in parallel between two large distribution channels with inlets A to D. The trigger channel volume of each cFET incrementally increases from right to left to create a full range of occluding bubble states. Inset shows a close-up illustrating how the trigger channel volume was incrementally increased by lengthening the trigger channels.

In these cases, the meniscus did not pin on the edges of the void volume due to a small leak. Despite this, there is a clear trend in the principal radii, and these outliers could be replaced with a linear interpolation of neighbouring points.

Based on this data, Eq. 4 can now be evaluated for a range of contact angles between $0°$ and $60°$, and trigger channel heights from $20\ \mu m$ to $150\ \mu m$. For calculation the pinch-off volume was set to 25.7 *nL*, the trigger channel width to $100\ \mu m$, the trigger channel length to 10 *mm*, water was the working fluid ($\eta = 8.9 \times 10^{-4}\ Pa.s,\ \gamma = 0.072\ N/m$), and air the working gas ($\eta = 1.872 \times 10^{-5}\ Pa.s$).[35] The main channel was 200 μm deep, and 0.8 mm long at the large opening.

A contour plot of the closing time is shown in Fig. 5a. The minimum closing time for this cFET main channel geometry is 11 ms. This closing time is achieved at a contact angle of $0°$ with a trigger channel depth of 115.8 μm (width of 100 μm). As can be observed from Fig. 5, there is a significant basin of values where the closing time is on the order of 100 *ms* or less. This demonstrates the robustness of the general operation of the cFET, with even non-optimal structures achieving good performance.

The results of the modelled closing time, compared to the previously reported experimental results[22] are shown in Fig. 5b. For a direct comparison, the model is re-calculated for a trigger channel length of 36 mm, and a contact angle of $0°$ to match the properties of the previous test device. While the agreement is reasonable, the model currently predicts generally faster closing than observed experimentally. In addition, the slowing of closing time due to high resistance or low capillary pressure trigger channels happens at a higher rate than experimentally observed. This disagreement can be explained by fabrication variation in the chip, distension of the hydrophobic cover into the channel, or deviations in the liquid surface tension and viscosity due to the addition of dye and stabilizing agents, the first two which can be reduced in the future through the use of more repeatable fabrication techniques such as injection molding and lamination.

It should also be stated, that, due to the discrete size of the *off*-valves included on the test chip, the data presented in Fig. 5 currently does not fully examine the available parameter space. Further improvements to the slew rate or closing time of the valve could be made by adjusting other aspects of the valve geometry. For example, examining the effect of the main channel geometry on closing time could yield further advances. This strategy could be particularly impactful, as the length and depth of the main channel will change both the main channel capillary pressure and pinch-off volume. Unfortunately, the ability to optimise the main channel is currently limited due to the lack of a method to determine the pinch-off volume and capillary back pressure analytically. At present, any main channel geometry must first be physically fabricated, tested, and analysed. However, as we demonstrate in the next section, this experimental approach still allows for a Shockley equation for cFETs to be developed.

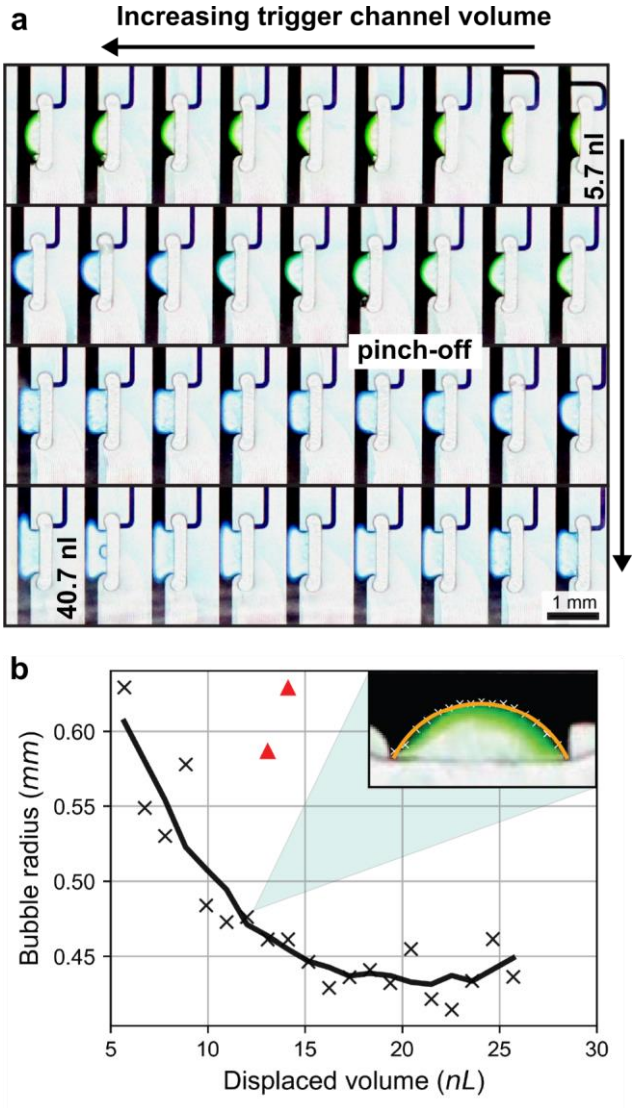

Fig. 4 The radius of the occluding bubble, as determined by the test device. **a** Optical micrographs showing the shape of the occluding bubble for 36 cFETs with trigger channel volumes varying from 5.7 nL to 40.7 nL (top to bottom, right to left). Occluding bubbles contact the main channel wall, and thus pinch-off fluid flow, at a volume of approximately 26 nL. The shape of these bubbles was used to calculate main channel capillary pressure as function of displaced volume. **b** Plot of the occluding bubble radius as a function of displaced volume. A circular arc was fitted to each meniscus/bubble shown in **a** using a gradient descent fitting algorithm. Each point represents the radius of an arc that was fitted to the meniscus shape. Outliers are indicated as red triangles. Inset shows an example of the circular arc fitting (line) against the extracted meniscus shape (X), overlaid onto an image of the meniscus.

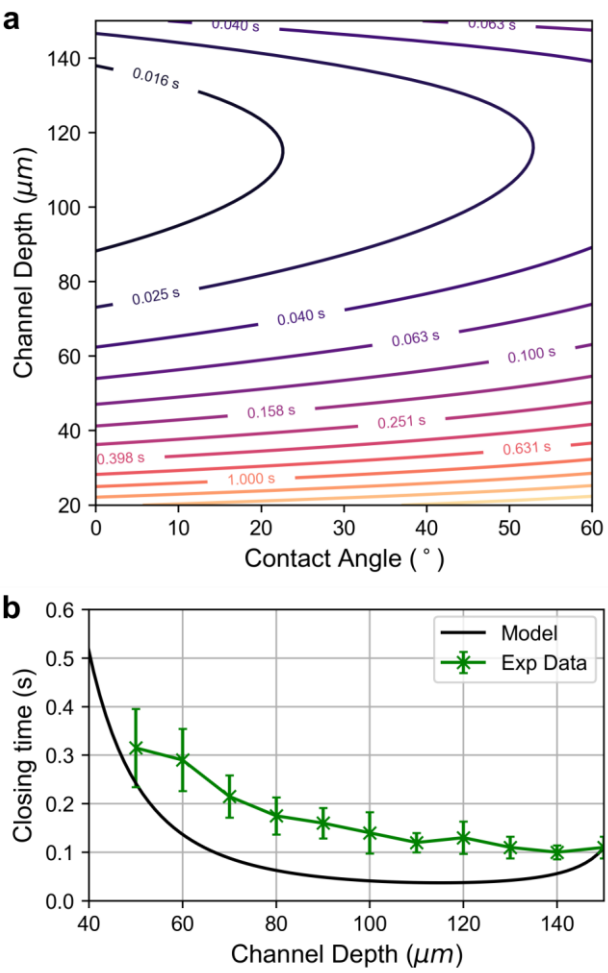

Fig. 5 The closing time of the cFET as a function of trigger channel depth and water contact angle. **a** Contour plot of the closing time. The trigger channel depth was evaluated from 20 to 150 μm and the contact angle from 0° and 60°. For the main channel geometry in this example (200 μm deep) the minimum closing time is approximately 11 milliseconds. **b** Results of the modelled closing time, compared to the previously reported experimental results.[22]

Shockley equation for capillaric-FETs

The Shockley equation is one of several fundamental equations that characterises the behaviour of electronic transistors.[27,28] It expresses the relationship between the current flowing through the main channel and the gate voltage applied, and is commonly written as,

$$i_D = i_{DSS}\left(1 - \frac{v_{GS}}{v_p}\right)^2, \qquad (5)$$

where i_D is the electronic current flowing through the drain, i_{DSS} the saturation current, v_{GS} the control voltage applied to the gate, and v_P the pinch-off voltage. The latter is the voltage at which the depletion region of the JFET completely occludes the main channel. As mentioned, a geometric parallel exists between the function of an electronic JFET, and the *off*-valve based cFET. Due to this, the Shockley equation should also describe the fluidic behaviour of the cFET, albeit with minor adjustments.

In an electronic JFET, the depletion region size is controlled by a potential energy (Voltage) applied to the gate.[27] In the case of the cFET, the position of the meniscus is controlled by the displaced volume in the trigger channel. The cFET allows volumetric fluid flow, rather than electronic current, to pass. For the cFET, therefore, the Shockley equation (Eq. 5) modifies to,

$$Q_D = Q_{ss}\left(1 - \frac{V_{tr}}{V_p}\right)^2, \qquad (6)$$

where Q_D is the flow rate through the main channel, Q_{ss} the saturation flow rate, V_{tr} the displaced trigger channel volume, and V_p the pinch-off volume. To determine the validity of this modified Shockley equation approach, the flow-rate - volume (Q-V) relationship of the cFET was experimentally examined, demonstrating that analogue resistance modes are controllable and achievable in this type of device.

To test the analogue resistance modes the same microfluidic device was used as for the characterisation of the transient dynamics. This is possible, as each unique bubble volume creates a different fluidic resistance for liquid flowing through the main channel. When a hydrostatic pressure is applied across the cFETs, flow will be induced proportional to the hydrostatic pressure applied and the size of the occluding bubble. On the test chip the cFETs are arranged in parallel between two large distribution channels. The large size of the distribution channels was chosen to minimize the driving pressure variation between transistors.

To initially fill the device, 105 µL of DI water, dyed blue, were loaded into a filling inlet (C or D inlets in Fig. 3) of the chip using a pipette. This filled the transistors with liquid and actuated the trigger channels for each device. The liquid did not flow into the top distribution channel because of the presence of a stop valve structure[1], which terminates each parallel transistor branch. Following filling, all remaining liquid was pipetted out of the filling inlet reservoir. To initiate fluid flow, 105 μL of DI water, dyed yellow was added to a testing Inlet (A or B inlets of Fig. 3). Liquid then flowed through each transistor branch proportional to the resistance of each parallel branch.

To better understand the potential effect of the distribution channels, the filling-testing cycle was repeated multiple times along both ordinal axes of the chip. For this, the device was filled with blue dye coloured water either from inlet C and tested by adding yellow coloured water to inlet B (*F*C*T*B), or from inlet D and tested by adding yellow coloured water to inlet A (*F*D*T*A). The flow rate induced by the pressure was measured by recording the change in colour through each transistor branch over time and subsequent analysis using ImageJ. The flow rate measurement was made at the beginning of the experiment, before any significant backpressure could develop at the outlet. This visual method of tracking the liquid flow rate was used as a stand in for a true volumetric flow rate measurement, which would be difficult to realize in the capillaric circuit.

An example of such an experimental result can be seen in Fig. 6**.** Video footage of this *F*C*T*B and an example *F*D*T*A experiment are provided in the ESI (V1). Because the parallel branches filled at a different rate, over the course of the experiment they also filled to a different extent. As such, the progression of the yellow colour along the individual parallel channels in Fig. 6 succinctly shows the controllability, and the general form, of the cFETs flow rate–trigger channel volume relationship. Now, using the time-based data, the extracted Q-V plot (analogous to an IV curve for a JFET) is shown in Fig. 7a. To obtain this graph, results were normalised as the hydrostatic driving pressure was uncontrolled in the experiment. In fact, this was deemed more useful, as it allowed the effect of the trigger channel volume and flow resistances to be shown – rather than the coupled effect of the trigger channels and driving pressure. In Fig. 7a, the *F*C*T*B test is shown in blue, and the *F*D*T*A test is shown in red. The mean of the recorded runs is illustrated as solid lines, with translucent lines indicating individual results, and the standard deviation of the measurement is given by the shaded regions.

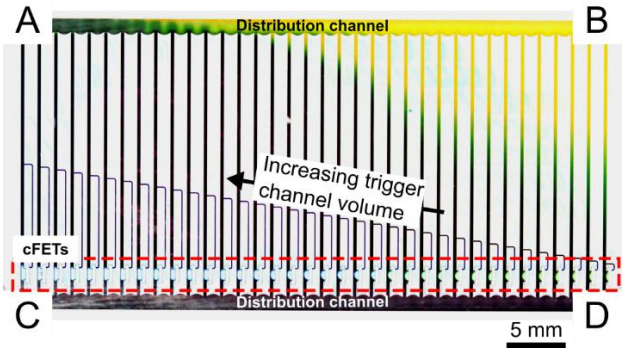

Fig. 6 Photograph showing the total liquid flow through the parallel resistor branches in proportion to the fluid resistance of the cFET devices. Labels indicate the testing (A,B) and filling (C,D) inlets. In this example the device was filled with blue dye coloured water from inlet C and tested by adding yellow coloured water to inlet B (FCTB). The image demonstrates the controllability in the resistance of the cFET devices.

Initial observation of Fig. 7a highlights two interesting phenomena. Firstly, the hydraulic resistance of the *off*-valves can be controlled by the applied trigger channel volume, in turn demonstrating that the analogue resistance of the cFET can be controlled. Secondly, there are three distinct regions of operation reproduced on this chip design. For small trigger channel volumes, the fluid flow is mostly restricted by external resistances on the chip, for example the resistances of the interconnecting channels. These are designed to be the same for all devices. For larger trigger channel volumes - approaching the pinch-off volume - fluid flow is being restricted by the increasing size of the occluding bubble. This creates a *hyperbolic* region where the flow resistance rapidly increases – a region described by the squared relationship of the Shockley equation (Eq. 6). On the other hand, for trigger channel volumes greater than the pinch-off volume, fluid flow in the cFET is completely restricted – this is the *cut-off* region.

To further illustrate this conceptual similarity, Fig. 7b shows the Shockley equation fitted to the data from the average of all the recorded data points. As can be observed in Fig. 7b, the Shockley equation provides a good fit for the experimental data in the *cut-off* and *hyperbolic* regions. In the low-volume regions, where the effect of external resistances is more pronounced, this fit breaks down, and the model and experimental data diverge. The point where the model diverges from the data is representative of when the external resistance becomes dominant over that of the cFET. This model fit also allow confirms the pinch-off volume, which was estimated in Fig. 4a. As expected, the flow-rate drops to zero after the observed pinch-off volume of 25.7 nL.

Figure 7 now allows the transconductance of a cFET to be defined for the first time, and approximate values to be calculated. In an electronic JFET, the transconductance is the rate of change of drain current, I_D, with respect to the gate-source voltage, V_{GS} at a constant drain source voltage.[36] This is the partial derivative of Eq. 5 with respect to V_{GS}. Therefore, the transconductance of a cFET is the change in main-channel flow rate, with respect to the change in displaced trigger channel volume at a constant hydrostatic pressure. This is the partial derivative of Eq. 6 with respect to displaced trigger channel volume. The maximum transconductance of this cFET was measured by fitting a linear line to the hyperbolic region, yielding $8.61 \pm 0.6\ nLs^{-1}\ nL^{-1}$ for the *F*D*T*A direction, and $36.8\ \pm 23.6\ nLs^{-1}nL^{-1}$ for the *F*C*T*B direction. The large variation between measurements is due to the uncontrolled hydrostatic testing pressure. Testing of the two diagonal directions on the chip (*FCTB, FDTA*) did not conclusively reveal an effect due to the pressure drop along the distribution channel. The driving pressure is a combination of the hydrostatic pressure, as well as the capillary pressure of the outlet meniscus. Due to this, any potential effect was dominated by the variation in total driving pressure. This cannot be eliminated using the current chip design, we anticipate that in the future the effect of the cFET alone can be determined by controlling the hydrostatic pressures applied, coupled with true volumetric flow measurements. Such measurements would also allow the effect of various cFET main channel geometries to be assessed.

Reversible operation of the cFET

The second criterion on which the original *off*-valves fell short of true transistor analogy, was their ability to oscillate. Capillary action devices are generally single use: Once a channel has been filled, the potential energy of the system has been expended, and no more liquid actuation can occur.[31] This in turn means that reversibility of any action within the system is difficult, if not impossible, and that reopening of the cFET by simply withdrawing liquid from the trigger channel will be difficult.

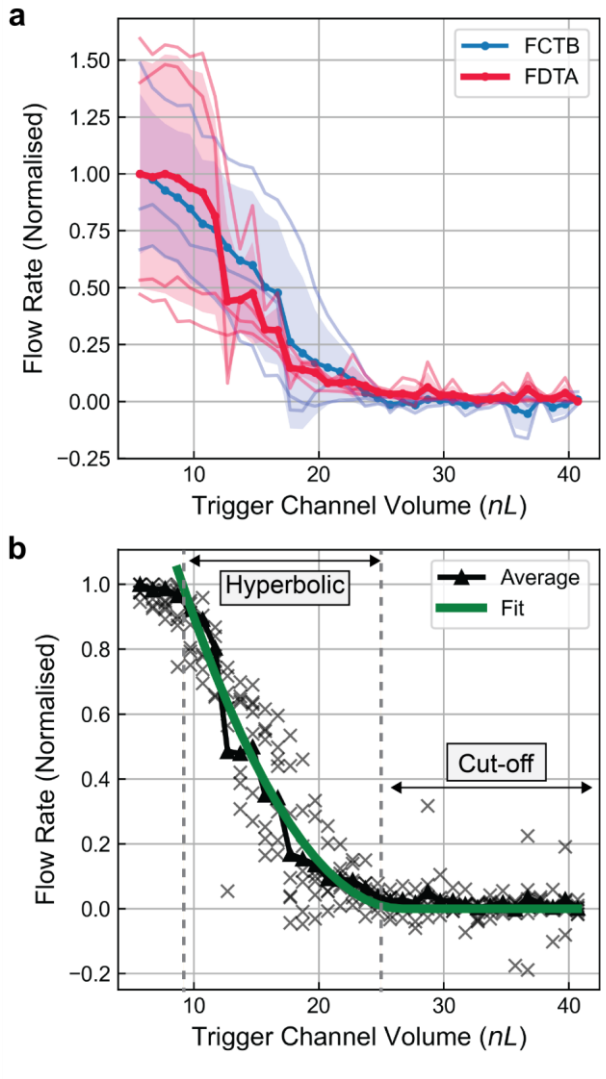

Fig. 7 Flow rate-volume (Q-V) relationship for the cFET device. **a** Plot of the Q-V relationship for the cFET device, as measured from the test chip. The chip was tested with a hydrostatic pressure applied between diagonally opposite pairs of inlets. This was done to visualize any potential influence of the distribution channels. The results are shown normalised to the mean response to illustrate the effect of the trigger channel volume more clearly. Devices were filled from inlet C and tested via inlet B (*FCT*B), or filled from D and tested via A (*FDTA*). **b** A Shockley equation form fitted to the Q-V response shown in **a**.

Interestingly, we found that the cFET can in fact operate reversibly, so long as there is still potential energy in the capillaric circuit and there is feedback void volume. This is possible because the bubble in the main channel of the device, in the closed or partially closed state, has its own capillary pressure. As such, the capillary pressure of the occluding bubble constitutes a restoring force that is balanced by the trigger channel pressure. If the capillary pressure of the trigger channel is mitigated, the volume is retracted, or if a vent is made available to the void volume- the cFET will re-open.

In this work, we present the simplest possible demonstration of this operation in the form of a vent being opened to the void volume of the transistor, allowing the cFET to re-open under its own restoring force. The chip utilised to experimentally demonstrate this was a modified version of a multiple-input NAND device reported previously (CAD files provided in the ESI).[26] This device consists of multiple trigger channels which lead into a single void volume. In its ordinary operation, the valve operates like a computational NAND function, completely closing only when all the trigger channels have been actuated.[26]

For the demonstration of re-opening, the inlets to all but one of the trigger channels were masked with semiconductor dicing tape, with the tape acting as a burstable membrane. In this configuration, any of the trigger channels will actuate the main channel of the cFET. Once the valve has been closed, a user then bursts one of the tape seals, for example by manually puncturing it with a syringe needle. The void volume is now able to vent through the burst membrane, and the restoring force created by the main channel meniscus will re-open the device. An experimental demonstration of this operation can be seen in Fig. 8. Video footage of this experiment is provided in the ESI (V2). At time-point t_1, the cFET was closed, with one trigger channel filled. This was followed by puncturing of the dicing tape on the inlet of channel 2 at t_2, leading to the valve reopening. At t_3, trigger channel 2 was filled to reclose the valve and reopened by puncturing the tape over channel 3 in t_4. This manual cycling was repeated one more time during $t_5$and t_6, with the possibility to extend this for as many times as required by the application. The total number of possible switching events is only limited by the number of vent channels which can physically be routed to the void volume.

Although this demonstration is relatively crude, it functionally demonstrates the reversibility of the cFET operation, providing a novel flow control pathway for relevant applications. For example, many biochemical assays require timed incubation steps.[22] Capillaric circuits generally manage the timing of incubation steps by use of long delay channels[2,37,38], however it may also be desirable to have user-controlled incubation periods. In such an application the cFET would be used to stop liquid progress using a feedback trigger channel and a user would manually resume fluid flow by bursting the tape membrane to vent the void volume. Evidently, there are other capillaric circuit elements which can also achieve such user actuated timing, the simplest example being a two-level trigger valve.[1] However, the potential advantage of using a cFET over a two-level trigger valve in this application would be for stability over longer incubation periods. For example, we have observed that the closed state of cFETs tends to be stable for 2 hours or more (see ESI, Fig. S2), which is significantly longer than the 15 to 30 minutes reported for conventional trigger valves.[39]

Ultimately though, as the goal of capillary circuits typically is to provide fully autonomous function, the integration of mechanically-moving parts, such as burstable membranes, is not necessarily a good fit due to their need for user intervention. Despite this, the experiments shown here demonstrate conclusively that the *off*-valve/cFET structure is fully capable of oscillation given an appropriate input. It would be conceivable to create automatic methods to achieve the same result using supporting capillaric circuitry. These could include using a capillary action retention valve[1] to remove liquid out of the trigger channel and connecting a lower flow resistance pump to the trigger channel.

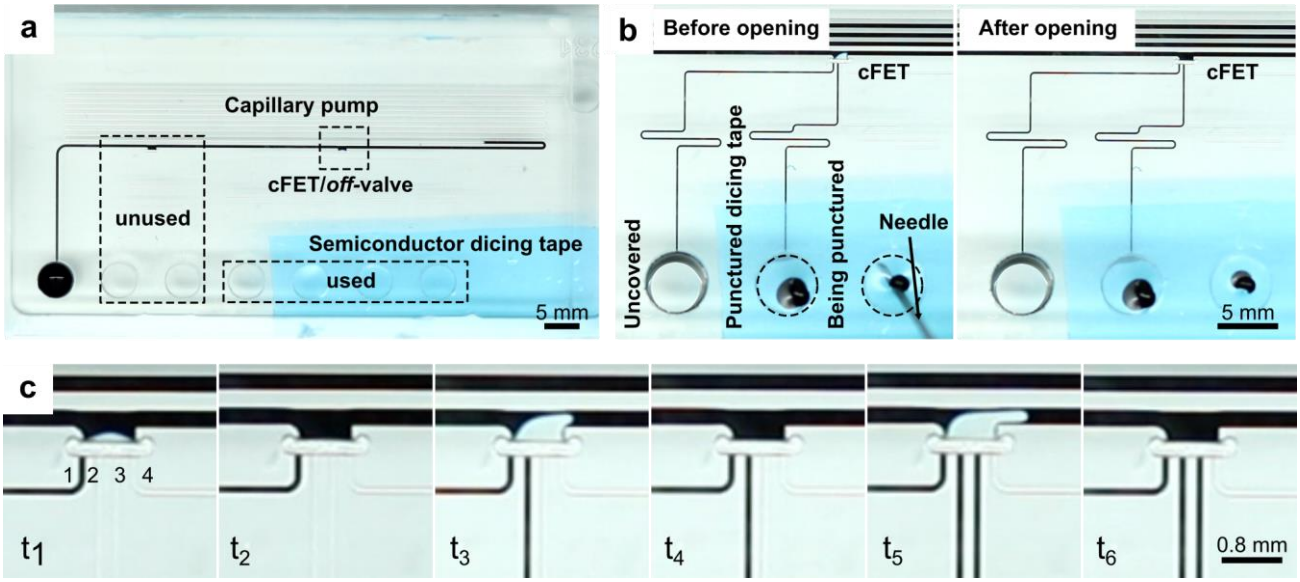

Fig. 8 Demonstration of the closing and re-opening of a cFET device by venting of the void volume. a Photograph of the capillary logic chip design[26] used for the reopening demonstration. A capillary pump actuates fluid flow through two *off*-valves/cFETs of which only the second valve is used for the demonstration. This second cFET has four trigger channels with externally accessible inlets. Three of these inlets are closed off with semiconductor dicing tape, providing an airtight seal. **b** Example of the switching between closed and reopened cFET states. Filled trigger channels 1 and 2 expand a bubble into the main channel (left). After the dicing tape covering channel 3 is punctured the bubble recovers, reopening the cFET (right). **c** Image sequence showing the bubble expansion and retraction over three transitions. At t_1 the cFET is shown in the closed state with only one trigger channel providing the volume. When trigger channel 2 is vented at $t_2 > t_1$ the cFET reopens. At t_3 the cFET is closed again with the help of trigger channel 2, and reopened at $t_4$by piercing the tape membrane over trigger channel 3. This transition is repeated a third time at t_5, closing the cFET again with the help of trigger channel 3, and reopened it at $t_6$via trigger channel 4. While the main purpose of this experiment was to show that the occluding bubble has a restoring force, and is able to re-open if required, it also illustrates that the volume of the actuating bubble is an adjustable function of the number of trigger channels.

3. Discussion

In this paper we have reported the first study of analogue resistance modes of a capillaric *off*-valve, providing support for the introduction of the term capillaric-FET, or cFET in short, for this type of structure. The capability of a cFET to actively control the flow resistance of a channel, as shown, represents a substantial functional addition to the capillaric circuit tool kit. Indeed, a wide range of applications in capillarics could profit from this kind of flow control. For example, the cFET could be used to control the stoichiometry of flowing reactants in a micro-fluidic channel, as already demonstrated in pressure-driven systems.[24] Traditionally, this would be controlled by the concentration of the input reactants, or by designing the size of the microchannels to obtain a specific flow resistance.[40] A cFET could not only achieve the same result as most of these solutions, but, more importantly, it could do so while also changing its resistance over time. For example, if the cFET was open initially, then actuated later in time, the ratio of reactants could be changed in a ramp or step function-like manner.

Based on the data shown here, natural limitations to the interoperability of the analogue resistance modes demonstrated remain. Currently the Q-V curve experiment shown in Fig. 7(a) does not control the hydrostatic pressure applied across the device as precisely as would be desirable. While, these results allowed us to conclude that the occluding bubble can be placed in a variety of states, thus producing a useful difference in flow resistance, due to the pressure drop along the distribution channel, and the driving pressure variation – we were not able to recreate a Q-V plot for a single device in isolation. Future work will thus seek to extend the physical characterisation of the structure. In particular, we aim to precisely control the applied pressure across the device and measure the fluid flow using conventional flow sensors, similar as has been done for pressure-driven systems.[24] Further study and prediction of the analogue resistance modes of the cFET, will establish this new type of flow-control device for a whole range of practical applications, thus enabling the realisation of previously incompatible assays on capillaric microfluidics platforms.

4. Materials and methods

Fabrication

Devices were fabricated from cross-linked polymethylmethacrylate (PMMA; 4.5 mm general purpose acrylic; PSP Plastics, Christchurch, New Zealand) as previously described.[22,26] Channel milling was performed using a Mini-Mill/GX micro milling machine running a NSK-3000 Spindle (Minitech Machinery Corporation, Norcross, GA, USA), with a minimum adressable step size of 1 µm. Machining tools were purchased from Performance Micro Tool (Janesville, WI, USA) in diameters of 3.175 mm (SR-4-1250-S), 250 µm (250M2X750S) and 100 µm (100M2X300S) for the square heads and 200 µm (TR-2-0080-BN) for the ball nose. Design files and milling parameters (G-code) were prepared using computer-aided design (CAD) software (Autodesk Fusion 360© 2020 Autodesk, Version 2.0.10356) for all functional units (CAD files provided in the ESI).

Each sample was fabricated by an initial face cut (3.175 mm cutter) to level out the surface, followed by milling of each channel. Milling shallower channels was carried out first to avoid burring on the edges, and all channel steps were repeated at bottom height at the end of milling to remove burrs. The surface was then polished using acrylic polish (aluminium oxide-based CRC, code 9230), followed by ultra-sonication for 1 min in ~5% (v/v) aqueous isopropyl alcohol solution, washing with acetone, isopropyl alcohol and water and blow drying with nitrogen. To close microscopic cracks that arose during the milling process, the surface was coated with high molecular weight PMMA solution (average Mw = 996,000, 2.5% in xylene; Sigma Aldrich, St Louis, MO, USA). Any remaining solvent was removed by drying samples at 90°C for 5 min on a hotplate and keeping the hot sample under vacuum for at least 1 min. Finally, samples were plasma-treated ten times for 1 min, each time at 25 W, pulsed mode (ratio 50) using oxygen gas (3 sccm; Tergeo Plasma Cleaner, Pie Scientific, Union City, CA, USA). A thin (2–3 mm) polydimethylsiloxane slab was prepared (PDMS; Sylgard 184, Electropar, NZ; mixed as given in instructions (10:1 w:w base:curing agent) and then cured at 80°C for 2h). This PDMS slab acted as a hydrophobic cover for the chip. A frame holder was used to ensure a tight seal of this to the PMMA channels. For the demonstration of re-opening, inlets on the PMMA were masked with semiconductor dicing tape (SWR 10+R, Nitto) and pierced with syringe needles.

Device Testing

All flow experiments were conducted by the addition of aqueous dye solutions (Brilliant Blue dye, #80717, Sigma Aldrich and Tartrazine, #T0388, Sigma Aldrich) into the reservoirs using a manual pipette. Liquid movement was recorded using a digital camera (Canon EOS 760D using a Canon Macro lens EF 100 mm 1:2.8 USM, recorded at 25 FPS). Images of the bubble shapes were binarized using ImageJ (FIJI)[41] and used to extract the shape of the bubble. A multivariate

gradient descent fitting algorithm could then be used to fit the origin and radius of a circular arc to the bubble. All data processing was performed using ImageJ, and Python 3.8[42] (Code provided in the ESI).

Author Contributions

C. M. and J. M. conceived the *off*-valve and cFET concept, C. M. fabricated the devices, performed experiments and analysed data. V. N. performed additional experiments. J. M. and D. M. performed additional analysis. C. M. wrote and revised the paper with input from J. M. F. D., D. M., C. F., R. D. and V. N. The work was supervised by R. D. and V. N.

Conflicts of interest

C. M., J. M., F. D., C. F., R. D., and V. N. are joint inventors on PCT/IB2021/051153, which covers the *off*-valve concept.

Acknowledgements

The authors would like to thank Helen Devereux and Gary Turner of the Nanofabrication Laboratory at the University of Canterbury for technical support. Funding was provided by MBIE Grant UOCX1706. V. N. acknowledges Rutherford Discovery Fellowship RDF-19-UOC-019 for additional funding.

References

1 Safavieh, R. & Juncker, D. Capillarics: pre-programmed, self-powered microfluidic circuits built from capillary elements. *Lab Chip* **13**, 4180-4189 (2013).

2 Olanrewaju, A., Beaugrand, M., Yafia, M. & Juncker, D. Capillary microfluidics in microchannels: from microfluidic networks to capillaric circuits. *Lab Chip* **18**, 2323-2347 (2018).

3 Juncker, D. et al. Autonomous Microfluidic Capillary System. *Anal. Chem.* **74**, 6139-6144 (2002).

4 Park, J., Han, D. H. & Park, J.-K. Towards practical sample preparation in point-of-care testing: user-friendly microfluidic devices. *Lab Chip* **20**, 1191-1203 (2020).

5 Sachdeva, S., Davis, R. W. & Saha, A. K. Microfluidic Point-of-Care Testing: Commercial Landscape and Future Directions. *Front. Bioeng. Biotechnol.* **8** (2021).

6 Salva, M. L., Rocca, M., Hu, Y., Delamarche, E. & Niemeyer, C. M. Complex Nucleic Acid Hybridization Reactions inside Capillary-Driven Microfluidic Chips. *Small* **16**, 2005476 (2020).

7 T. U, V., Ghosh, S., Milleman, A., Nguyen, T. & Ahn, C. H. A new polymer lab-on-a-chip (LOC) based on a microfluidic capillary flow assay (MCFA) for detecting unbound cortisol in saliva. *Lab Chip* **20**, 1961-1974 (2020).

8 Li, Y. et al. A distance-based capillary biosensor using wettability alteration. *Lab Chip* **21**, 719-724 (2021).

9 Ma, B. et al. Wearable capillary microfluidics for continuous perspiration sensing. *Talanta* **212**, 120786 (2020).

10 Hemmig, E., Temiz, Y., Gökçe, O., Lovchik, R. D. & Delamarche, E. Transposing Lateral Flow Immunoassays to Capillary-Driven Microfluidics Using Self-Coalescence Modules and Capillary-Assembled Receptor Carriers. *Anal. Chem.* **92**, 940-946 (2020).

11 Hassan, S.-u. & Zhang, X. Design and Fabrication of Capillary-Driven Flow Device for Point-Of-Care Diagnostics. *Biosensors* **10**, 39 (2020).

12 Hassan, S.-u. et al. Capillary-Driven Flow Microfluidics Combined with Smartphone Detection: An Emerging Tool for Point-of-Care Diagnostics. *Diagnostics* **10**, 509 (2020).
13 Ghosh, S. et al. A new microchannel capillary flow assay (MCFA) platform with lyophilized chemiluminescence reagents for a smartphone-based POCT detecting malaria. *Microsys. Nanoeng.* **6**, 5 (2020).
14 Che, C. et al. Activate capture and digital counting (AC + DC) assay for protein biomarker detection integrated with a self-powered microfluidic cartridge. *Lab Chip* **19**, 3943-3953 (2019).
15 Epifania, R., Soares, R. R. G., Pinto, I. F., Chu, V. & Conde, J. P. Capillary-driven microfluidic device with integrated nanoporous microbeads for ultrarapid biosensing assays. *Sens. Actuators, B* **265**, 452-458 (2018).
16 Olanrewaju, A. O., Ng, A., DeCorwin-Martin, P., Robillard, A. & Juncker, D. Microfluidic Capillaric Circuit for Rapid and Facile Bacteria Detection. *Anal. Chem.* **89**, 6846-6853 (2017).
17 Liu, D. et al. A fully integrated distance readout ELISA-Chip for point-of-care testing with sample-in-answer-out capability. *Biosens. Bioelec.* **96**, 332-338 (2017).
18 Delamarche, E., Temiz, Y., Lovchik, R. D., Christiansen, M. G. & Schuerle, S. Capillary Microfluidics for Monitoring Medication Adherence. *Ang. Chem., Int. Ed.* http://dx.doi.org/10.1002/anie.202101316 (2021).
19 Olanrewaju, A. O., Robillard, A., Dagher, M. & Juncker, D. Autonomous microfluidic capillaric circuits replicated from 3D-printed molds. *Lab Chip* **16**, 3804-3814 (2016).
20 Hitzbleck, M. et al. Capillary soft valves for microfluidics. *Lab Chip* **12**, 1972-1978 (2012).
21 Arango, Y., Temiz, Y., Gökçe, O. & Delamarche, E. Electro-actuated valves and self-vented channels enable programmable flow control and monitoring in capillary-driven microfluidics. *Sci. Adv.* **6**, eaay8305 (2020).
22 Menges, J. et al. New flow control systems in capillarics: off valves. *Lab Chip* **21**, 205 – 214 (2020).
23 Gao, Y., Wu, M., Lin, Y. & Xu, J. Trapping and control of bubbles in various microfluidic applications. *Lab Chip* **20**, 4512-4527 (2020).
24 Khoshmanesh, K. et al. A multi-functional bubble-based microfluidic system. *Sci. Rep.* **5**, 9942 (2015).
25 Zhou, Y. et al. Standing Air Bubble-Based Micro-Hydraulic Capacitors for Flow Stabilization in Syringe Pump-Driven Systems. *Micromachines* **11**, 396 (2020).
26 Meffan, C. et al. (2021) Transistor off-Valve Based Feedback, Metering and Logic Operations in Capillary Microfluidics. IEEE 34th International Conference on Micro Electro Mechanical Systems (MEMS), Virtual, 218-221.
27 Shockley, W. A Unipolar "Field-Effect" Transistor. *Proc. IRE* **40**, 1365-1376 (1952).
28 Dacey, G. C. & Ross, I. M. Unipolar "Field-Effect" Transistor. *Proc. IRE* **41**, 970-979 (1953).
29 Vourdas, N., Moschou, D. C., Papadopoulos, K. A., Davazoglou, D. & Stathopoulos, V. N. A new microfluidic pressure-controlled Field Effect Transistor (pFET) in digital fluidic switch operation mode. *Microelectronic Eng.* **190**, 28-32 (2018).
30 de Wijs, W.-J. A., Laven, J. & de With, G. Wetting forces and meniscus pinning at geometrical edges. *AIChE J.* **62**, 4453-4465 (2016).

31 Narayanamurthy, V. et al. Advances in passively driven microfluidics and lab-on-chip devices: a comprehensive literature review and patent analysis. *RSC Adv.* **10**, 11652-11680 (2020).
32 Kirby, B. Micro- and nanoscale fluid mechanics: transport in microfluidic devices. (Cambridge University Press, 2010).
33 Mikaelian, D. & Jones, B. Modeling of capillary-driven microfluidic networks using electric circuit analogy. *SN Appl. Sci.* **2**, 415 (2020).
34 Bruus, H. Theoretical Microfluidics (Oxford Univ. Press, 2008).
35 Rumble, J. (ed) CRC Handbook of Chemistry and Physics (CRC Press Boca Raton, 2020).
36 Sedra, A. S. & Smith, K. C. Microelectronic circuits (Oxford Univ. Press, 2015).
37 Gervais, L. & Delamarche, E. Toward one-step point-of-care immunodiagnostics using capillary-driven microfluidics and PDMS substrates. *Lab Chip* **9**, 3330-3337 (2009).
38 Gervais, L., Hitzbleck, M. & Delamarche, E. Capillary-driven multiparametric microfluidic chips for one-step immunoassays. *Biosens. Bioelec.* **27**, 64-70 (2011).
39 Zimmermann, M., Hunziker, P. & Delamarche, E. Valves for autonomous capillary systems. *Microfluid. Nanofluid.* **5**, 395-402 (2008).
40 deMello, A. J. Control and detection of chemical reactions in microfluidic systems. *Nature* **442**, 394-402 (2006).
41 Schindelin, J. et al. Fiji: an open-source platform for biological-image analysis. *Nat. Meth.* **9**, 676-682 (2012).
42 Rossum, G. V. & Drake, F. L. Python 3 Reference Manual. (CreateSpace, 2009).